A Particle-Particle Simulation Model for Droplet Acceleration in Colloid Thrusters

IEPC-2019-526

Presented at the 36th International Electric Propulsion Conference
University of Vienna, Austria
September 15-20, 2019

Yinjian Zhao* and Joseph J. Wang†
University of Southern California, Los Angeles, California, 90089, USA

We present a Particle-Particle (PP) model for simulating droplet acceleration in a colloid thruster. This model explicitly models each individual droplet as a spherical particle with a finite radius, calculates the electrostatic force between each droplet pair directly from the Coulomb's law, and eliminates the typical constrains from mesh resolution and domain size from a particle-mesh based approach. The model is first validated against both the analytical solution and 3-D particle-in-cell simulations of 1-D space charge flow. Then, the model is applied to simulate a typical colloid thruster using CH_3NO as propellant. Simulation results show that droplet acceleration is dominated by the interactions between droplet and the applied electrostatic field, as expected, and the modification from droplet space charge on the applied electric field is minimum. Due to both the large initial droplet acceleration by the electric field at the Taylor cone tip and the 3-D beam effect. the current that can be transmitted by charged droplets in a colloid thruster can be orders of magnitude larger than the space charge limit predicted by the 1-D Child-Langmuir law.

I. Introduction

Colloid thrusters are valued for their high thrust density, high specific impulse, and high efficiency, and can provide the extremely precise propulsion capability required for many small spacecraft based missions[7]. Droplet acceleration is one of the most fundamental aspects in colloid thruster design and operation. While there have been extensive colloid thruster developments in recent years, the understanding of droplet acceleration is still limited due to the difficulties involved to accurately measure the process and a lack of accurate numerical simulation models[5].

The ion acceleration process in electric thrusters has been modeled extensively using the particle-in-cell (PIC) model[10−14]. However, PIC[15] may not be the most efficient method for simulating droplet acceleration. To model the droplet acceleration process, one needs to resolve both highly collisional region near the Taylor cone tip and the more rarefied region near the extractor. As the size of the Taylor cone jet is much smaller than the characteristic scale of the acceleration region, a PIC model would require the use of an extremely fine mesh resolution near the Taylor cone[16,17], thus leading to significant computation time/resource spent on solving the electrostatic field. Moreover, the limitations of using macro-particles to represent finite-sized droplets in a PIC approach are also unknown. Thus, we are motivated to explore a different simulation approach.

This paper presents a simulation study of droplet acceleration using the Particle-Particle (PP) model[9,18]. In this model, each individual droplet is explicitly modeled as a particle with a finite size, and the Coulomb interactions between droplets are calculated directly from the Coulomb's law between each particle pair. Typically, the PP method is not as computationally efficient as PIC because its computing time scales as N^2, where N is the number of particles in the simulation. However, since the PP approach does not use a mesh system and thus eliminates the computations related to particle-mesh interpolation and solving the

*PhD Student, Astronautical Engineering, yinjianz@usc.edu.
†Professor, Astronautical Engineering, josephjw@usc.edu

elliptical Poisson's equation, it can be computational advantageous for those applications with constrains from mesh resolution and domain size. Moreover, the PP simulation algorithm is simple and straightforward. When implemented using shared-memory parallel computing techniques, the simulation can be speeded up significantly and the parallel efficiency can be extremely high, especially with the utilization of GPU accelerators.

This paper is organized as follows. Sec.II presents the PP simulation model. Sec. III compares the PP simulation against analytical solution and PIC simulation of a 1-D space charge flow as well as PP simulation against PIC simulation of a 3-D beam. Sec. IV presents a PP simulation study on droplet acceleration with a focus on the space charge effect. Sec. V contains a summary and a discussion of future study.

II. The PP Simulation Model

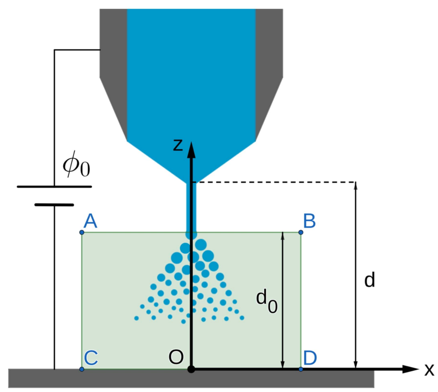

Figure 1. Schematic diagram of a colloid thruster and the simulation domain.

The simulation model focuses on the droplet acceleration region between the propellant needle outlet and the accelerator grid (shown by the green shaded region ($ABDC$) in Fig. 1. In Fig. 1, the origin of the coordinate system is the point O on the accelerator gird surface, the z-axis is the symmetric axis of the needle pointing toward the needle outlet), d denotes the distance from the tip of the Taylor cone to the accelerator grid, and d_0 denotes the distance from the location where the jet breaks to the accelerator grid.

In this model, droplet extraction from the accelerator grid is not modeled due to the very different sizes between the accelerator region and the holes on the grid. The extractor grid is treated as a transparent surface. Droplets that pass through the grid are deleted from the simulation. Note that the PP model does not use a mesh system and thus does not have a domain boundary in the radial direction.

The current carried by the ionic liquid jet I can be obtained from[1]

$$I = f(\varepsilon)(\frac{\gamma K \dot{V}_j}{\varepsilon})^{1/2}, \tag{1}$$

where ε is relative permittivity, K the conductivity, γ the surface tension, $\dot{V}_j$ the volume flow rate, and $f(\varepsilon)$ an empirical parameter[1], $f(\varepsilon) \simeq 18$ for $\varepsilon > 40$. We assume that the liquid jet is a cylinder with a radius R_j, and all the droplets are spherical ones. The droplets that break up directly from the jet have a radius R_d. R_d and R_j are related from[2,3]

$$R_j = \frac{R_d}{1.89} = \frac{r^*}{1.89}[\frac{3}{f(\varepsilon)}]^{2/3}, \tag{2}$$

where ε_0 is the vacuum permittivity, and $r^* = (\varepsilon\varepsilon_0\dot{V}_j/K)^{1/3}$ is the "characteristic dimension" of the cone-jet transition region[2,3]. Note that Eq. (2) uses the factor 3 instead of 6 because experiments have shown that the droplets produced by electrospray streams are charged to about 1/2 of their Rayleigh limit. From these assumptions, the droplets broken off from the jet have a volume of $V_d = 4\pi R_d^3/3$, an emission rate of $\dot{N}_d = \dot{V}_j/V_d$, a charge of $Q_d = I/\dot{N}_d$, and a mass of $M_d = \rho V_d$.

During each simulation time step Δt, the droplets are injected one by one into the simulation domain.

We consider that all the droplets have the same initial axial velocity as that of the jet

$$v_d = \frac{\dot{V}_j}{\pi R_j^2}. \tag{3}$$

In the simulation, the injected droplets are randomly placed in an cylindrical injection volume, which has a height $H = v_d \Delta t$ from the jet front, and a radius R_j. The positions of the injected droplets are set to be random inside the injection volume:

$$\begin{aligned} x &= R_j \sqrt{U} \sin(2\pi U'), \\ y &= R_j \sqrt{U} \cos(2\pi U'), \\ z &= d_0 - U'' H, \end{aligned} \tag{4}$$

where U, U', and U'' are three independent random numbers uniformly distributed in the interval $(0, 1)$. The droplet breakup during the flow is not considered in this work.

The droplet dynamics is described by

$$M_d \frac{d^2 \boldsymbol{r}}{dt^2} = M_d \frac{d\boldsymbol{v}}{dt} = \boldsymbol{F} = \boldsymbol{F}_{pp} + \boldsymbol{F}_{acc} = Q_d(\boldsymbol{E}_{pp} + \boldsymbol{E}_{acc}), \tag{5}$$

The force $\boldsymbol{F}$ on a droplet includes two contributions: $\boldsymbol{F}_{pp}$ is the Coulomb force due to all other droplets, and $\boldsymbol{F}_{acc}$ is the electrostatic force from the applied external electric field. $\boldsymbol{E}_{pp}$ and $\boldsymbol{E}_{acc}$ denote the electric field due to the charges from other droplet and the applied field at the droplet location, respectively. The equation of motion is integrated using the Verlet algorithm[4].

The electric field due to all other droplets at the location of the ith droplet is calculated from

$$\boldsymbol{E}_{pp}^{(i)} = \frac{Q_d}{4\pi\varepsilon_0} \sum_{j=1, j\neq i}^{N} \frac{\boldsymbol{r}_{ij}}{|\boldsymbol{r}_{ij}|^3}, \quad |\boldsymbol{r}_{ij}| \geq 2R_d \tag{6}$$

where $\boldsymbol{r}_{ij}$ is the distance vector pointing from the center of the jth droplet to that of the ith droplet, and N denotes the total number of simulated droplets at that time. Since all the droplets in the acceleration region are positively charged and we assume that the droplets do not undergo deformation, the center-to-center distance between any droplet pairs in the simulation is always larger than $2R_d$.

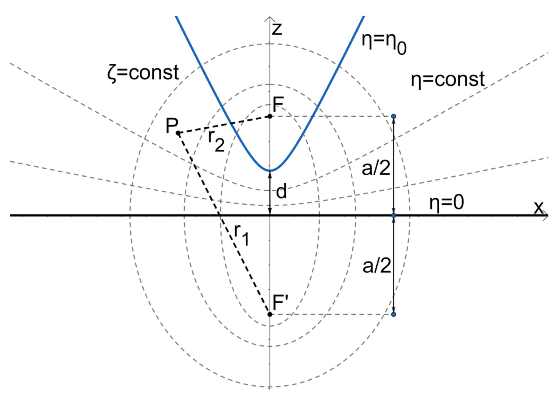

Figure 2. The prolate spheroidal coordinate system used for the analytical solution of the Taylor cone.

Fig. 2 shows the prolate spheroidal coordinate, (ζ, η, φ), used to solve the applied electric field involving a Taylor cone. Here

$$\begin{aligned} \zeta &= (r_1 + r_2)/a, \\ \eta &= (r_1 - r_2)/a, \end{aligned} \tag{7}$$

$$\begin{aligned} r_1 &= [x^2 + y^2 + (z + a/2)^2]^{1/2}, \\ r_2 &= [x^2 + y^2 + (z - a/2)^2]^{1/2}, \end{aligned} \tag{8}$$

where a is the half focal length of the hyperboloids, and φ is the azimuthal angle about the line FF'. In the simulation model, the surface $\eta = 0$ represents the accelerating plate, and the surface $\eta = \eta_0$ represents the liquid surface, i.e. the Taylor cone surface.

We take the potential on the Taylor cone surface ($\eta = \eta_0$) to be a constant $\phi_{acc} = \phi_0$, and the potential on the accelerating plate ($\eta = 0$) to be $\phi_{acc} = 0$. Then the solution for ϕ_{acc} will only depend on η.

$$\phi_{acc}(\eta) = \phi_0 \frac{\tanh^{-1}\eta}{\tanh^{-1}\eta_0}. \tag{9}$$

The values of a and η_0 can be determined from

$$a = 2d(1 + R_c/d)^{1/2}, \qquad \eta_0 = (1 + R_c/d)^{-1/2}, \tag{10}$$

where the radius of curvature is $R_c = R_n/\cos\theta_T$, R_n is the needle radius, the Taylor cone angle is $\theta_T = 49.29°$. The electric field can then be solved from

$$\boldsymbol{E}_{acc} = -\boldsymbol{\nabla}\phi_{acc} = -(\frac{\partial\phi_{acc}}{\partial\eta}\frac{\partial\eta}{\partial x}, \frac{\partial\phi_{acc}}{\partial\eta}\frac{\partial\eta}{\partial y}, \frac{\partial\phi_{acc}}{\partial\eta}\frac{\partial\eta}{\partial z}) \tag{11}$$

Fig. 3 shows the potential of the applied field (i.e. the field when no charged droplets are present) used for later simulations.

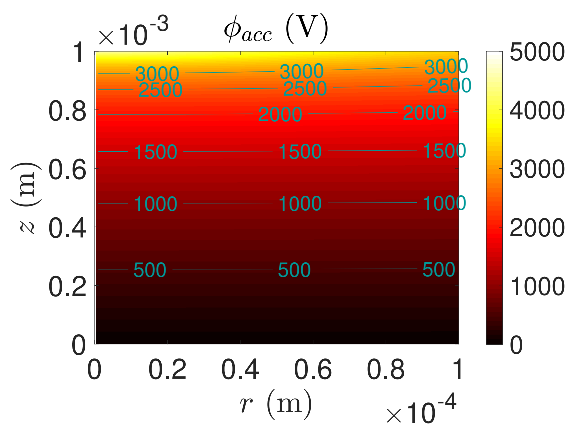

Figure 3. The applied accelerating potential used in the simulation.

III. Model Validation

A. Code Validation: 1-D Space Charge Flow

1. *The Child-Langmuir Law*

We first validate the model by considering a simple 1-D space charge flow between two parallel electrodes with a gap d and a potential difference ϕ_0. At the space charge limit, the current that can be transmitted between the electrodes is given by he Child-Langmuir law[6].

$$J_{SCL} = \frac{4}{9}\varepsilon_0\sqrt{\frac{2e}{m}}\frac{\phi_0^{3/2}}{d^2}, \tag{12}$$

If the flow is along the z direction from $z = 0$ to $z = d$, and the potential at $z = 0$ is $\phi(0) = 0$, the potential distribution is given by

$$\phi(z) = \left(\frac{3}{2}\right)^{4/3}\left(\frac{J_{SCL}}{\varepsilon_0}\right)^{2/3}\left(\frac{m}{2e}\right)^{1/3} z^{4/3}. \tag{13}$$

The electric field distribution is

$$E_z(z) = -\frac{4}{3}\left(\frac{3}{2}\right)^{4/3}\left(\frac{J_{SCL}}{\varepsilon_0}\right)^{2/3}\left(\frac{m}{2e}\right)^{1/3} z^{1/3}. \tag{14}$$

2. The PIC Model

First, we apply a 3D PIC model to simulate the space charge flow in a cubic domain. The fixed potential boundary condition (Dirichlet) is applied on $z = 0$ and $z = d$, $\phi(0) = 0$, $\phi(d) = \phi_0$. Those particles that travel out of the domain in the z direction are deleted. The periodic boundary condition is applied on x and y directions for both the field and particles.

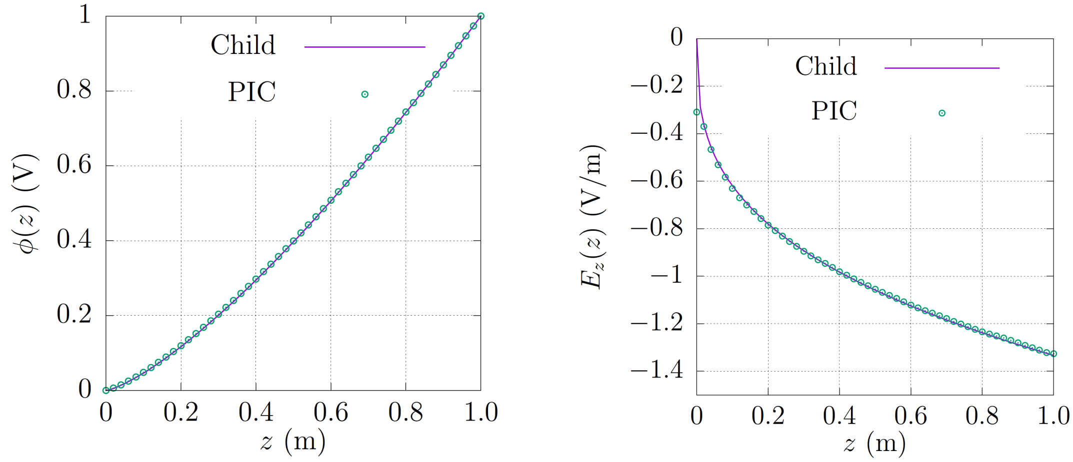

Figure 4. The potential distribution (left), the electric field distribution (right).

The parameters used are as follows. The potential difference is $\phi_0 = 1$ V. The separation of the two plates is $d = 1$ m, which is the length of the simulation domain in z direction. So, the constant electric field without space charge effect is $E_0 = \phi_0/d = 1$ V/m. The length of the simulation domain in x and y directions are also set to be d. Thus the simulation domain is a cubic box. The simulated particles are electrons with charge $-e$ and mass m, $e = 1.6 \times 10^{-19}$ C, $m = 9.1 \times 10^{-31}$ kg. The resultant space-charge-limited current density is $J_{SCL} \approx 2.332$ μA/m^2.

We consider the emission of an electron beam with $J = -J_{SCL}$. The potential distribution and the electric field distribution from the PIC simulation is shown in Fig. 4. In the plot, the potential and the electric field are averaged using all grid points in x and y along z. Fig. 4 shows the PIC result matches well against the analytical solution.

3. The PP Model

Next, we consider the PP model. The simulation parameters and the electron injection are the same as that in the PIC model. For particles that travel out of the domain in x or y direction, we still apply the periodic boundary condition.

One numerical issue in the PP method is that two macro-particles may approach very close to each other within one simulation time step, thus resulting in a nonphysically large Coulomb?s force. This is not an issue for the droplet simulation because the droplet are finite-sized particles. When PP is applied to the simulation of electrons, the implementation of the Coulomb must be modified in the short range. The approach is to consider that macro-particles rep[resenting electrons are also finite-sized rather than point particles and apply a cut-off in the Coulomb force between the electrons when the positions between two electrons overlap. This cutoff model was also used previously in a work to simulate ion beam neutralization[18].

Fig. 5 compares the potential and the electric field distribution along the center line for PP, PIC, and the analytical solution. The three solutions generally matches well, although there is a small deviation in the PP result. We believe the small deviation may be a result of two factors. The first is the cut-off in the field model described above. The second is that the PP model does not naturally allow a periodic boundary condition and thus the implementation of the periodic boundary condition in the model is somewhat artificial.

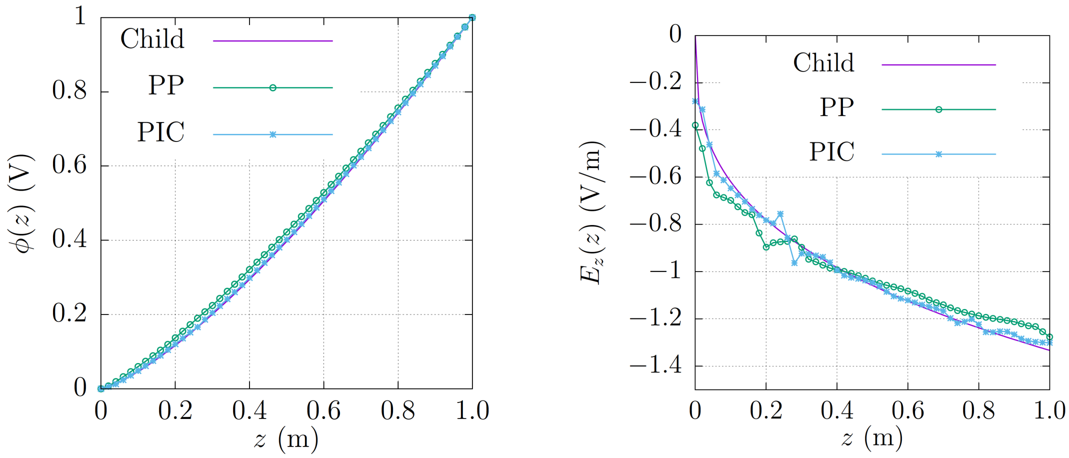

Figure 5. The potential distribution (left), the electric field distribution (right).

B. PIC vs. PP: 3-D Beam

We next compare PIC and PP on the simulation of a 3-D beam. We consider the injection of electrons from a circular emission surface centered at $(0.5, 0.5, 0)$ m on the $z = 0$ plane, and with a radius $R = 0.25$ m. We still choose the emitted current density $J = -J_{SCL}$, thus the current changes to $I = J\pi R^2 \approx -0.458$ μA. Other parameters are still the same, except those that are related to the current will be changed accordingly.

Fig. 6 shows the PIC and PP simulation results of the potential and electric field distributions. For comparison, the 1-D Child-Langmuir law is also plotted. We find that PP and PIC match each other. However, the electron beam diverges due to the space charge of the beam. Hence, the Child-Langmuir law does not apply in this case.

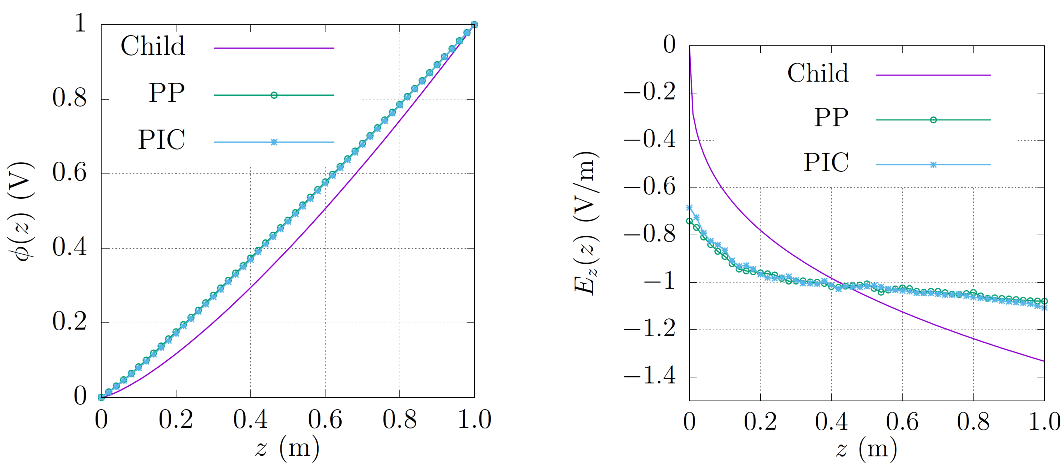

Figure 6. The potential distribution (left), the electric field distribution (right).

Fig. 7 further shows the magnitude contour of the electric field component E_z in the $y = 0.5$m plane. Overall the PP results match with that of PIC. However, the electron beam expansion in the PP result is slightly larger than that in PIC. Again, this is because the force cut-off model used in the PP is not exactly the same as that in PIC.

IV. PP Simulations of Droplet Acceleration

The simulation results presented here consider a colloid thruster using CH_3NO as the propellant. The parameters for the propellant and specific thruster design are shown in Tab. 1. Here, we assume that the jet

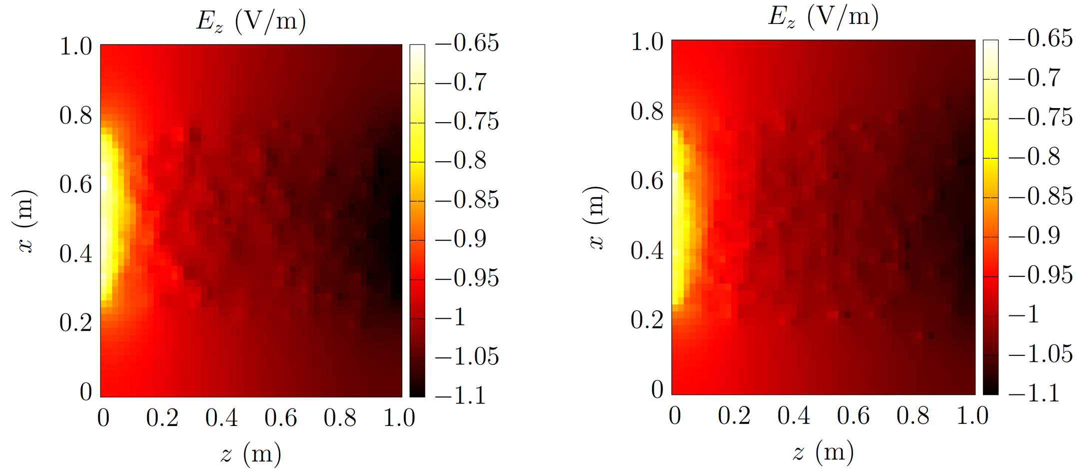

Figure 7. The electric field distribution of PIC (left), the electric field distribution of PP (right).

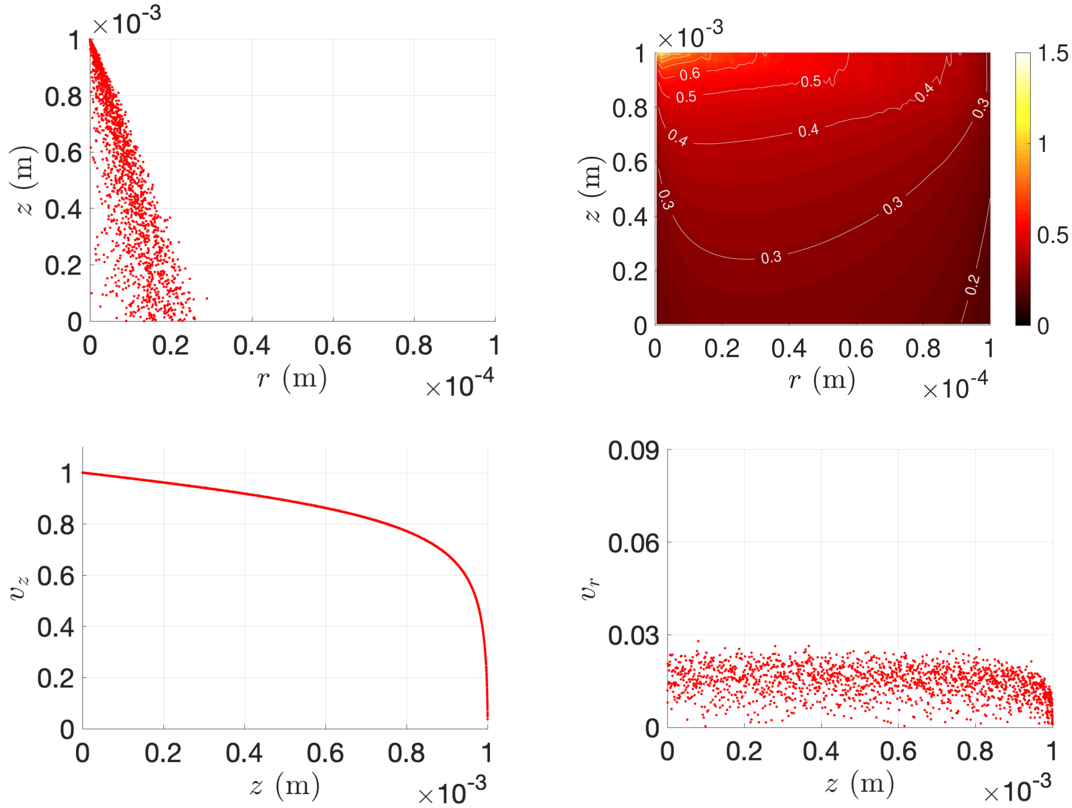

Figure 8. Top left: r-z spatial plot of droplets. Top right: Potential in volts only due to droplets. Bottom left: z-v_z phase space plot of droplets. Bottom right: z-v_r phase space plot of droplets. v_z and v_r are normalized by the expected final speed $(2Q_d\phi_0/M_d)^{1/2}$.

breaks into droplets immediately at the Taylor cone tip for simplicity. This assumption is reasonable because the characteristic length L of the cone-jet transition region is much less than the length of the acceleration region[5]: $L \approx 2R_0\dot{V}_j/\dot{V}_0 \approx 24.22$ nm $\ll d_0$, where $2R_0 = [\gamma\varepsilon_0^2/(\rho K^2)]^{1/3}$, $\dot{V}_0 = \gamma\varepsilon_0/(\rho K)$. Hence, in the simulations presented in this paper, $d = d_0$. Based on the propellant and thruster design parameters in Tab. 1, the other physical parameters for simulation input can be calculated and are shown in Tab. 2.

The simulation results are shown in Fig. 8. From the r-z spatial plot, we can see the beam expands

Propellant Parameters	
Conductivity	$K = 1$ S/m
Relative permittivity	$\varepsilon = 100$
Surface tension	$\gamma = 0.059$ N/m
Mass density	$\rho = 1130$ kg/m^3
Empirical current factor	$f(\varepsilon) = 18$
Thruster Parameters	
Volume flow rate	$\dot{V}_j = 7 \times 10^{-15}$ m^3/s
Needle radius	$R_n = 15$ μm
Distance between needle tip and accelerator grid	$d = 1$ mm
Distance between jet front and accelerator grid	$d_0 = 1$ mm
Accelerating voltage	$\phi_0 = 5$ kV

Table 1. Propellant and thruster parameters

Current	$I = 36.58$ nA
Cone-jet transient dimension	$r^* = 18.37$ nm
Jet radius	$R_j = 2.94$ nm
Droplet radius	$R_d = 5.56$ nm
Droplet mass	$M_d = 8.15 \times 10^{-22}$ kg
Droplet charge	$Q_d = 3.77 \times 10^{-18}$ C
Droplet initial speed	$v_d = 257.18$ m/s
Droplet emission rate	$\dot{N}_d = 9.71 \times 10^9$ s^{-1}
Radius of curvature	$R_c = 19.79$ μm
Half focal length	$a = 2.02$ mm
Taylor cone parameter	$\eta_0 = 0.99$

Table 2. Physical parameters for simulation input

radially while being accelerated along the $-z$ direction. From the z-v_z phase space plot, we can see that all droplets are accelerated mainly in the upstream region near the jet, due to the strong accelerating electric field there. The z-v_r phase space plot is also shown, which indicates that droplets gain their final radial velocity around $z = 0.8$ mm, and after that they expand with a constant radial velocity. Therefore, the particle-particle interactions (collisions) near the jet dominates the radial expansion. The potential distribution due to the space charge of droplets is also shown, from which we can see the magnitude is only about 1.5 V based on the mesh resolution (100×100) used to generate this plot.

It is interesting to compare the emitted current with the 1-D space charge limit current emission. In this simulation, the emitted current is $I = 36.58$ nA, the jet radius is $R_j = 2.94$ nm, thus the emitted current density is $J = I/(\pi R_j^2) \approx 1.344 \times 10^9$ A/m^2. Using the droplet charge $Q_d = 3.77 \times 10^{18}$ C, mass $M_d = 8.15 \times 10^{-22}$ kg. accelerating potential $\phi_0 = 5000$ V, and the tip-to-plate distance $d_0 = 1$ mm. the 1-D space charge limit current is

$$J_{SCL} = \frac{4}{9}\varepsilon_0 \sqrt{\frac{2Q_d}{M_d}} \frac{\phi_0^{3/2}}{d_0^2} \approx 133.8 \quad \text{A/m}^2.$$

Hence, the emitted current density is seven orders of magnitude larger than J_{SCL}. However, the simulation result shows that the space charge effect is minimum in the beam.

One reason for this is that the droplets are emitted from the tip of the Taylor cone. The electric field at the Taylor cone tip is about $E_T = 8.506 \times 10^7$ V/m. This electric field provides a large initial acceleration to the droplet than the electric field at the surface of a planar electrode. Another reason is the 3-D effect. Due to the extremely small radial size and beam expansion, the Child-Langmuir law derived from 1-D space charge flow obviously does not apply in the situation considered here.

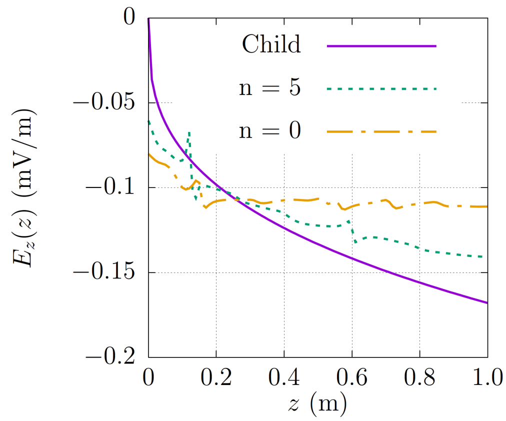

Figure 9. The electric field distribution.

One way to evaluate the difference between a 1D and a 3D beam is to apply the image charges in the 3D PP simulation. When calculating the Coulomb field, some image charges in the x and y directions are also involved. The electric field at the location of the ith particle $\boldsymbol{E}_{pp}^{(i)}$ can be evaluated from

$$\boldsymbol{E}_{pp}^{(i)} = \frac{1}{4\pi\varepsilon_0} \sum_{\boldsymbol{n}} \sum_{j=1}^{N}{}' \frac{q_j(\boldsymbol{r}_i - \boldsymbol{r}_j + \boldsymbol{n}L)}{|\boldsymbol{r}_i - \boldsymbol{r}_j + \boldsymbol{n}L|^3}, \tag{15}$$

where L is the domain length in the x and y direction, $\boldsymbol{n}L = n_1 L\hat{x} + n_2 L\hat{y}$ denotes an arbitrary repeat vector, n_1 and n_2 are arbitrary integers, the $'$ symbol is to exclude the term $j = i$ if and only if $\boldsymbol{n} = \boldsymbol{0}$. This calculation refers to the basics of Ewald summation[21,22].

To illustrate the 3-D effects, we rerun the droplet acceleration simulation with a reduced acceleration potential of 0.1mV and a reduced macro-particle weight of $N_W \approx 2.46$. All other parameters are kept the same. We use Eq. (15) to evaluate the electric field E_z along the z-axis, on 100 uniformly distributed points from $z = 0$ to $z = 1$ m. The electric field distribution of two runs are plotted in Fig. 9. The curve of $n = 0$ is a run without the image particles, while the curve of $n = 5$ is a run with five image particles in each of the x, $-x$, y, and $-y$ directions. Namely, for every simulated particle, there are 10×10 corresponding image particles. From Fig. 9, we can see that a larger n leads to a E_z distribution that is closer to the Child-Langmuir law. In the $n = 0$ run, i.e. the 3D situation, the space charge effects are much less than that in the 1D situation.

V. Summary and Conclusions

A Particle-Particle (PP) model is developed to simulate droplet acceleration in a colloid thruster. The PP model explicitly models each individual droplet as a spherical particle with a finite radius, and calculates the electrostatic force between each droplet pair directly from the Coulomb's law. Simulation results confirm the expected droplet acceleration process in a colloid thruster. The droplet acceleration is dominated by the interactions between droplet and the applied electrostatic field, as expected. The space charge modification on the applied electric field is minimum. In a colloid thruster, the current that can be transmitted by charged droplets can be orders of magnitude larger than the space charge limit predicted by the 1-D Child-Langmuir law. This is due to both the large initial droplet acceleration by the electric field at the Taylor cone tip and the 3-D beam effect.

Future study will investigate droplet acceleration in other operation regimes and further exam the space charge effects. Future work will need to explicitly model the droplet breakup process and droplet extraction from the accelerator grid. Additionally, more cross-comparisons between this PP model and other relevant PIC models are also needed.

Acknowledgments

The simulations in this paper were performed at the Center for High-Performance Computing of the University of Southern California.

References

[1]J. Mora, F., and Loscertales, I. G., "The Current Emitted by Highly Conducting Taylor Cones", Journal of Fluid Mechanics, Vol. 260, pp. 155-184, 1994.

[2]Martinez-Sanchez, M., and Lozano, P., "16.522 Space Propulsion", Massachusetts Institute of Technology: MIT OpenCourseWare, License: Creative Commons BY-NC-SA, Spring 2015.

[3]Rayleigh, L., "XX. On the Equilibrium of Liquid Conducting Masses Charged with Electricity", The London, Edinburgh, and Dublin Philosophical Magazine and Journal of Science, Vol. 14, pp. 184-186, 1882.

[4]Verlet, L., "Computer Experiments on Classical Fluids. I. Thermodynamical Properties of Lennard-Jones Molecules", Physical Review, Vol. 159, pp. 98, 1967.

[5]Gañán-Calvo, A. M., López-Herrera, J. M., Herrada, M. A., Ramos, A., and Montanero, J. M., "Review on the Physics of Electrospray: From Electrokinetics to the Operating Conditions of Single and Coaxial Taylor Cone-jets, and AC Electrospray", Journal of Aerosol Science, Vol. 125, pp. 32-56, 2018.

[6]Umstattd, R. J., Carr, C. G., Frenzen, C. L., Luginsland, J. W., and Lau, Y. Y., "A Simple Physical Derivation of Child–Langmuir Space-charge-limited Emission using Vacuum Capacitance", American Journal of Physics, Vol. 73, No. 2, pp. 160-163, 2005.

[7]Rossi, C., "Micropropulsion for Space - A Survey of MEMS-based Micro Thrusters and their Solid Propellant Technology", Sensors Update, Vol. 10, pp. 257-292, 2002.

[8]Taylor, S. G., "Disintegration of Water Drops in an Electric Field", Proceedings of the Royal Society A, Vol. 280, pp. 383-397, 1964.

[9]Hockney, R. W., and Eastwood, J. W., "Computer Simulation using Particles", IOP Publishing Ltd, 1988.

[10]Hu, Y., and Wang, J., "Fully Kinetic Simulations of Collisionless Mesothermal Plasma Emission: Macroscopic Plume Structure and Microscopic Electron Characteristics", Physics of Plasmas, Vol. 24, pp. 035510, 2017.

[11]Wang, J., Chang, O., and Cao, Y., "Electron-ion Coupling in Mesothermal Plasma Beam Emission", IEEE Transactions on Plasma Science, Vol. 40, pp. 230-236, 2012.

[12]Liu, H., Wu, B., Yu, D., Cao, Y., and Duan, P., "Particle-in-cell Simulation of a Hall Thruster", Journal of Physics D: Applied Physics, Vol. 43, pp. 165202, 2010.

[13]Taccogna, F., Longo, S., Capitelli, M., and Schneider, R., "Particle-in-cell Simulation of Stationary Plasma Thruster", Contributions to plasma physics, Vol. 47, pp. 635-656, 2007.

[14]Zhao, Y., Liu, H., Yu, D., Hu, P., and Wu, H., "Particle-in-cell Simulations for the Effect of Magnetic Field Strength on a Cusped Field Thruster", Journal of Physics D: Applied Physics, Vol. 47, pp. 045201, 2014.

[15]Birdsall, C., and Langdon, A., "Plasma Physics via Computer Simulation", McGraw-Hill, New York, 1985.

[16]Wang, P., Borner, A., Korkut, B., Li, Z., and Levin, D., "Simulations of Electrospray in a Colloid Thruster with a High Resolution Three-dimensional Particle-in-Cell Model", 44th AIAA Plasmadynamics and Lasers Conference, AIAA 2013-2629, 2013.

[17]Wang, P., Borner, A., Li, Z., and Levin, D., "An Advanced Particle-in-cell (PIC) Approach for Electrospray Simulation in a Colloid Thruster using Molecular Dynamics Simulation Results", 43rd AIAA Thermophysics Conference, AIAA 2012-2993, 2012.

[18]Zhao, Y., Wang, J., and Usui, H., "Simulations of Ion Thruster Beam Neutralization using a Particle–particle Model", Journal of Propulsion and Power, Vol. 34, pp. 1109-1115, 2018.

[19]Lozano, P., and Martnez-Sanchez, M., "Studies on the Ion-droplet Mixed Regime in Colloid Thrusters", PhD dissertation, MIT, Department of Aeronautics and Astronautics, 2003.

[20]Carretero-Benignos, J. A., and Martnez-Sanchez, M., "Numerical Simulation of a Single Emitter Colloid Thruster in Pure Droplet Cone-jet Mode", PhD dissertation, MIT, Department of Aeronautics and Astronautics, 2005.

[21]Ewald, P. P., “The calculation of optical and electrostatic grid potential”, ANNALEN DER PHYSIK, Vol. 64, pp. 253-287, 1921.

[22]Pfeifer, R. J., and Hendricks, C. D., “Charge-to-Mass Relationships for Electrohydrodynamically Sprayed Liquid Droplets” The Physics of Fluids, Vol. 10, No. 10, pp. 2149-2154, 1967.